JOURNAL OF SCIENCE AND TECHNOLOGY
ISSN: 2229-8460 e-ISSN: 2600-7924

JST

Vol. 16 No. 1 (2024) 10-22
https://publisher.uthm.edu.my/ojs/index.php/jst

The Effect of a Riga Plate On Casson Hybrid Nanofluid Flow Along a Stretching Cylinder with an Exponential Heat Source and Thermal Radiation

Adekunle Aworinde[1], Silas Oseme Okuma[2]*, Adeisa Olusegun Areo[1], Mariam Ololade Akande[3], Peter Adegbite[1], Akintayo Oladimeji Akindele[1]

[1] *Department of Pure and Applied Mathematics, Ladoke Akintola University of Technology, Ogbomoso, NIGERIA*
[2] *Department of Mechanical Engineering, Nigeria Maritime University, Okerenkoko, NIGERIA*
[3] *Department of Physical and Chemical Science, Federal University of Health Science, Ila Orangun, NIGERIA*

*Corresponding Author: silasoseme@gmail.com
DOI: https://doi.org/10.30880/jst.2024.16.01.002

Article Info

Received: 8 February 2024
Accepted: 23 May 2024
Available online: 23 June 2024

Keywords

Riga plate, exponential heat source, hybrid nanofluid, thermal radiation, drug delivery

Abstract

This study investigates the effect of a Riga plate on the flow characteristics of a Casson hybrid nanofluid through a stretching cylinder embedded in a porous medium in the presence of an exponential heat source and thermal radiation. This model is used to explore the potential applications of this analysis in the fields of cancer treatment and wound healing. The governing partial differential equations are converted into a system of nonlinear ordinary differential equations using suitable similarity transformations. The governing partial differential equations (PDEs) were reduced to ordinary differential equations (ODEs) using similarity variables, and the heat transfer phenomena, fluid flow dynamics, and nanoparticle behavior in the base fluid were captured through numerical analysis. The Casson fluid model was used to capture the non-Newtonian characteristics of blood-like fluids in the circulatory system, and stretching was employed to mimic the blood vessel. The modeling involved incorporating thermal radiation (Ra) and an exponential heat source, which are encountered in cancer treatment. The Runge-Kutta order 4 with shooting technique was used to obtain numerical solutions of the governing equations, and the effects of the Casson fluid parameter, curvature parameter, nanoparticle volume fraction, Eckert number, and radiation parameter were analyzed. The results showed that the Riga plate affected the flow patterns by increasing the temperature, and the temperature distribution was improved by increasing the radiation parameter and nanoparticle concentration. The insights from this study could be used to optimize heat-based treatments for cancer and wound healing, where control of fluid dynamics and heat transfer processes is critical.

1. Introduction

The analysis of hybrid nanofluid flow and heat transfer in composite systems such as biological organs and machine parts is crucial in numerous engineering and industrial applications. The essential area of hybrid

nanofluids, where the behavior of traditional fluids is improved by the addition of hybrid nanoparticles. The application of hybrid nanofluids, which is suspensions of two or more nanoparticles in conventional base fluids, has gained significant attention due to their enhanced thermal conductivity and heat transfer properties [1]. This improved fluid property is important in Casson fluid such as blood. The Casson fluid model, known for encompassing non-Newtonian characteristics such as shear-thinning behavior, adds complexity to the fluid dynamics, making it a fascinating subject for investigation [2-5]. The presence of a Riga plate, a common feature in many industrial processes, introduces additional complexities to the Casson hybrid nanofluid flow field along a stretching cylinder. Understanding how the Riga plate influences the flow characteristics of the Casson hybrid nanofluid is crucial for optimizing processes and designing efficient systems [6-10].

Moreover, the inclusion of an exponential heat source and thermal radiation adds further layers of interesting application, reflecting real-world scenarios where heat generation and radiation play pivotal roles in system performance [11-15]. The enhanced thermal conductivity of fluid can be put in use in science and engineering.

Researchers have tirelessly dedicated their efforts to improving the thermophysical properties of fluid flow for cancer treatment. Most cancerous cells originate in the epithelium, which lines the body's internal organs and is supplied with blood through cylindrical blood vessels on their surfaces. Detecting cancer at its early, treatable stages before it invades deeper tissues or spreads is challenging [16]. The New Optical Probe technique, based on light-scattering spectroscopy (LSS), can detect precancerous and early cancerous changes in cell-rich epithelia. This study explores the use of hybrid nanofluids to treat early-stage tissue invasion by cancer cells through computational fluid dynamics analysis of their behavior in stretched cylinders on a surface.

Hybrid nanofluids, a new generation of fluids, have gained attention from bio scientists and medical practitioners due to their enhanced thermophysical properties like dynamic viscosity, electrical conductivity, and thermal conductivities. They excel in applications where thermal and electrical conductivities are crucial, such as in nanomedicine, where they can help control malignant growth in patients by delivering electrically conducting hybrid nanofluid-based treatments involving radiation and drugs. Nanotechnology, which involves mixing nanosized micro-objects with base fluids, allows efficient drug distribution within the human body, enabling precise targeting of cells and tissues [17]. This field of science has opened new avenues for research and applications, including the exploration of unique fluid characteristics such thermal conductivity [18] by incorporating nanoparticles like gold and copper nanoparticles.

These technological advancements have gained significant attention in the field of medicine. Park et al. [19] created the anti-cancer drug Doxorubicin (DOX) by using micellar hybrid nanoparticles that contained magnetic nanoparticles (MN) and quantum dots (QD). These long-circulating micellar hybrid nanoparticles (MHNs) with magnetic iron oxide nanoparticles (MNs) and quantum dots (QDs) serve as anticancer drugs. They enable drug delivery, dual mode near infrared (NIR) fluorescence imaging, and MRI of diseased tissue in vitro and in vivo. Zhou et al. [20] conducted a study on iron oxide hybrid nanoparticles with a core-shell structure, exploring controlled synthesis to biomedical applications. Jun et al. [22] discovered that biologically important components like DNA, antibodies, and peptides can be easily attached to magnetic nanoparticles, creating versatile nano-bio hybrid particles with both magnetic and biological functions for biomedical diagnostics and therapeutics. Ahmad et al. [21] investigated the unique properties of hybrid nanofluids, including manganese zinc ferrite ($MnZnFe_2O_4$) and nickel zinc ferrite ($NiZnFe_2O_4$), in bio-convective flow of motile gyrostatic microorganisms in a Darcy-Forchheimer medium. They also considered the activation energy's impact. Soares et al. [23] highlighted the ongoing advances in biomedical applications of polymer-hybrid nanoparticles.

Tripathi et al. [24] employed unsteady hybrid nanoparticle-mediated magneto-hemodynamics and heat transfer in a simulation of drug delivery through an overlapped stenotic artery. Bhatti and Abdelsalam [25] studied the peristaltic propulsion of hybrid nanofluid flow with Tantalum (Ta) and Gold (Au) nanoparticles under magnetic effects, considering the Hartmann number and thermal Grashof number. Chahregh and Dinarvand analyzed hybrid nanofluid stagnation point flow on a stretching surface with heat transfer, noting the superior thermal properties of hybrid nanofluids [26]. Awais et al. [29] investigated the magneto-hydrodynamic (MHD) effect on ciliary-induced peristaltic flow with rheological hybrid nanofluid, aiming to provide a more realistic approach to cancer treatment using hybrid nanoparticles and induced magnetic fields in endoscopy.

Researchers [28-29] explored various aspects of hybrid nanofluid behavior. Additionally, Waga et al. [36] studied magneto-Burgers nanofluid stratified flow with swimming motile microorganisms and dual-variable conductivity configured by a stretching cylinder or plate. Research also observed that the shape factor affects fluid flow on a cylindrical surface, as discussed by [31–35]. Also, the influence of the electric field and couple stress Casson hybrid nanofluid was analyzed by [36–41] and the findings indicate that hybrid nanoparticles can help maintain normal blood temperature and improve heat transfer rates. Furthermore, the engineering and manufacturing sectors have shown interest in analyzing non-Newtonian fluids like Casson fluid due to its extensive applicability, as explained by Casson's rheological model for non-Newtonian liquid flow developed in 1995[42-52]. However, this present investigates the effect of a Riga plate on Casson hybrid nanofluid flow along a stretching cylinder with an exponential heat source and thermal radiation.

J. of Science and Technology Vol. 16 No. 1 (2024) p. 10-22

2. Mode Formulation

The incompressible Casson flow isotropic equation given as follows:

$$\tau_{ij} = \begin{cases} 2\left(\mu_B + \frac{P_y}{\sqrt{2\pi}}\right)e_{ij}, & \pi > \pi_c \\ 2\left(\mu_B + \frac{P_y}{\sqrt{2\pi_c}}\right)e_{ij}, & \pi < \pi_c \end{cases} \tag{1}$$

Where, τ_{ij} , μ_B , P_y , $\pi = e_{ij}e_{ij}$, $e_{ij} = (i,j)th$, π_c are respectively the Stress tensor, Non-Newtonian fluid dynamic viscosity , Fluid yield stress of the liquid, product of the rate of strain tensor with tensor, component of the deformation rate, critical value of the product based on the non-Newtonian model
Considering steady, 2-dimensional laminar Casson hybrid nanofluid through a stretching cylinder embedded in Darcy-Forchiemer porous medium. The riga plate with current density j_0 is place above the stretched cylinder to provide modified magnetic field. The hybrid nanoparticles which is mixture of Radium and alumina nanoparticle in base fluid is introduced [54]. The cylinder stretched with stretching velocity $u_w = \frac{bx}{l}$, where l *and* b characteristics length and velocity respectively. The concentration equation is ignored due to addition of the hybrid nanoparticles, the sedimentation and coagulation effect the hybrid nanoparticles and blood is assumed to be negligible The fluid is set a motion along r-direction with surface temperature T and free stream temperature T_∞ . Moreover, non-uniform exponential heat/sink source is applied. The detailed geometry is shown in Figure 1. The governing equations are given [30].

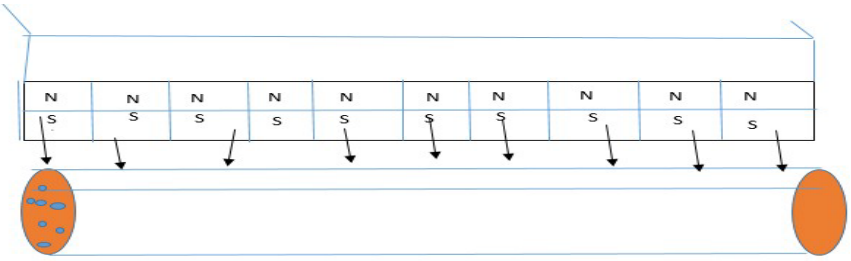

Fig. 1 *Flow geometry*

$$\frac{\partial(ru)}{\partial x} + \frac{\partial(rv)}{\partial r} = 0 \tag{2a}$$

$$u\frac{\partial u}{\partial x} + v\frac{\partial u}{\partial r} = \frac{\nu_{hnf}}{r}\left(1+\frac{1}{\delta}\right)\frac{\partial}{\partial r}\left(r\frac{\partial u}{\partial r}\right) + \frac{\pi j_0 M_0}{8\rho_{hnf}}e^{\frac{\pi}{a}x} - \frac{\nu_{hnf}}{K_p}u + g\beta(T-T_0) \tag{2b}$$

$$u\frac{\partial T}{\partial x} + v\frac{\partial T}{\partial r} = \frac{\alpha_{hnf}}{r}\frac{\partial}{\partial r}\left(r\frac{\partial T}{\partial r}\right) + \frac{\mu_{hnf}}{(\rho C_p)_{hnf}}\left(1+\frac{1}{\delta}\right)\left(\frac{\partial u}{\partial r}\right)^2 - \frac{\partial q_r}{\partial r} + q'' \tag{3}$$

Here $(u\ ,v)$ is the fluid velocity along, $(x\ ,r)$, $\nu_{hnf}, \delta, \sigma_{hnf}, \rho_{hnf}, j_0, M_0, a, g, \beta_T, K_p$ is the hybrid nanofluid kinematics viscosity, the Casson fluid parameter, electrical conductivity of the hybrid nanofluid, density of the hybrid hybrid nanofluid, the electric field strength, magnetic field strength, current density, magnetization of the magnet, with of the electrode, gravitational acceleration , volume expansivity and porosity respectively.

The boundary conditions following [37].

$$\begin{cases} r = a, u = u_w(x) = b\dfrac{x}{l}, v = 0, T = T_w(x) + T_0\left(\dfrac{x}{l}\right)^n \\ r = \infty, T \to T_\infty, u \to 0 \end{cases} \tag{4}$$

The non-uniform heat source following [40] is given as:

$$q''' = \left(\frac{k_{hnf} u_w}{x \nu_{hnf}}\right)\left[A\left(T_w - T_\infty + \right)f' + B\left(T - T_\infty\right)\right] \tag{5}$$

Where A is space dependent heat generation/absorption parameter and B means temperature dependent heat generation/absorption parameter. If $A < 0$ and $B < 0$ denote the internal heat sink also, if $A > 0$ and $B > 0$ represent the internal heat generation. The radiative heat flux q_r followed [19] and [20] is defined by

$$\frac{\partial q_r}{\partial r} = 4\left(T - T_\infty\right)\Gamma \tag{6}$$

Γ is absorption coefficient

Table 1 *Thermo-physical properties of hybrid base fluid and nanoparticles*

Physical properties	$C_2H_6O_2$	Ra	Al_2O_3
$\rho\left(\frac{kg}{m^3}\right)$	1113.5	5000	3950
$C_p\left(\frac{J}{kg \cdot k}\right)$	2430	120	451
$k\left(\frac{W}{m \cdot k}\right)$	0.253	18.6	12

Thermos-physical properties of the hybrid Nano Fluid is giving as follow

$$\nu = \frac{\mu_{hnf}}{\rho_{hnf}} \tag{7}$$

$$\frac{\mu_{hnf}}{\rho_{hnf}} = \frac{\mu_f}{\rho_f\left(\left(1-\varphi_2\right)\left(1-\varphi_1+\varphi_2\left(\frac{\rho_{s1}}{\rho_f}\right)\right)+\varphi_2\rho_{s2}\left(1-\varphi_1\right)^{2.5}\left(1-\varphi_2\right)^{2.5}\right)} \tag{8}$$

Let

$$\varepsilon_1 = \rho_f\left(\left(1-\varphi_2\right)\left(1-\varphi_1+\varphi_2\left(\frac{\rho_{s1}}{\rho_f}\right)\right)+\varphi_2\rho_{s2}\left(1-\varphi_1\right)^{2.5}\left(1-\varphi_2\right)^{2.5}\right) \tag{9}$$

$$\mu_{hnf} = \frac{\mu_f}{\left(1-\varphi_1\right)^{2.5}\left(1-\varphi_2\right)^{2.5}} \tag{10}$$

J. of Science and Technology Vol. 16 No. 1 (2024) p. 10-22

$$\varepsilon_2 = \left(1-\varphi_1\right)^{2.5}\left(1-\varphi_2\right)^{2.5} \tag{11}$$

$$\rho_{hnf} = \rho_f\left(\left(1-\varphi_2\right)\left(1-\varphi_1+\varphi_2\left(\frac{\rho_{s1}}{\rho_f}\right)\right)+\varphi_2\rho_{s2}\right) \tag{12}$$

$$\varepsilon_3 = \left(\left(1-\varphi_2\right)\left(1-\varphi_1+\varphi_2\left(\frac{\rho_{s1}}{\rho_f}\right)\right)+\varphi_2\rho_{s2}\right) \tag{13}$$

$$k_{hnf} = k_f * \frac{k_{s1}+(m-1)k_f-(m-1)\varphi_1\left(k_f-k_{s1}\right)}{k_{s1}+(m-1)k_f+\varphi_2\left(k_f-k_{s1}\right)} * \left(\frac{\mathrm{k_{s2}}+\mathrm{k_f}\,(\mathrm{m}-1)\left(\frac{k_{s1}+(m-1)k_f-(m-1)\varphi_1\left(k_f-k_{s1}\right)}{k_{s1}+(m-1)k_f+\varphi_1\left(k_f-k_{s1}\right)}-(\mathrm{m}-1)\phi_2\left(k_f\left(\frac{k_{s1}+(m-1)k_f-(m-1)\varphi_1\left(k_f-k_{s1}\right)}{k_{s1}+(m-1)k_f+\varphi_1\left(k_f-k_{s1}\right)}\right)-k_{s2}\right)\right)}{\mathrm{k_{s2}}+(\mathrm{m}-1)\mathrm{k_f}\left(\frac{k_{s1}+(m-1)k_f-(m-1)\varphi_1\left(k_f-k_{s1}\right)}{k_{s1}+(m-1)k_f+\varphi_1\left(k_f-k_{s1}\right)}\right)+\varphi_2\left(k_f\left(\frac{k_{s1}+(m-1)k_f-(m-1)\varphi_1\left(k_f-k_{s1}\right)}{k_{s1}+(m-1)k_f+\varphi_1\left(k_f-k_{s1}\right)}\right)-k_{s2}\right)}\right) \tag{14}$$

$$\varepsilon_4 = \frac{k_{s1}+(m-1)k_f-(m-1)\varphi_1\left(k_f-k_{s1}\right)}{k_{s1}+(m-1)k_f+\varphi_2\left(k_f-k_{s1}\right)} * \left(\frac{\mathrm{k_{s2}}+\mathrm{k_f}\,(\mathrm{m}-1)\left(\frac{k_{s1}+(m-1)k_f-(m-1)\varphi_1\left(k_f-k_{s1}\right)}{k_{s1}+(m-1)k_f+\varphi_1\left(k_f-k_{s1}\right)}-(\mathrm{m}-1)\phi_2\left(k_f\left(\frac{k_{s1}+(m-1)k_f-(m-1)\varphi_1\left(k_f-k_{s1}\right)}{k_{s1}+(m-1)k_f+\varphi_1\left(k_f-k_{s1}\right)}\right)-k_{s2}\right)\right)}{\mathrm{k_{s2}}+(\mathrm{m}-1)\mathrm{k_f}\left(\frac{k_{s1}+(m-1)k_f-(m-1)\varphi_1\left(k_f-k_{s1}\right)}{k_{s1}+(m-1)k_f+\varphi_1\left(k_f-k_{s1}\right)}\right)+\varphi_2\left(k_f\left(\frac{k_{s1}+(m-1)k_f-(m-1)\varphi_1\left(k_f-k_{s1}\right)}{k_{s1}+(m-1)k_f+\varphi_1\left(k_f-k_{s1}\right)}\right)-k_{s2}\right)}\right) \tag{15}$$

$$\left(\rho Cp\right)_{hnf} = \left(\rho Cp\right)_f\left(\left(1-\varphi_2\right)\left(1-\varphi_1+\varphi_1\frac{\left(\rho Cp\right)_{s1}}{\left(\rho Cp\right)_f}\right)+\varphi_2\left(\rho Cp\right)_{s2}\right) \tag{16}$$

$$\varepsilon_5 = \left(\left(1-\varphi_2\right)\left(1-\varphi_1+\varphi_1\frac{\left(\rho Cp\right)_{s1}}{\left(\rho Cp\right)_f}\right)+\varphi_2\left(\rho Cp\right)_{s2}\right)\left(\rho Cp\right)_{hnf} = \varepsilon_5\left(\rho Cp\right)_f \tag{17}$$

The similarity variables (16) were introduced following [27-40] to reduce Equations (2) and (3) into ODEs

$$\begin{cases}\psi = \left(\nu_f x u_w\right)^{\frac{1}{2}} a f\left(\eta\right), u = \dfrac{1}{r}\dfrac{\partial\psi}{\partial r} \\ u = -\dfrac{1}{r}\dfrac{\partial\psi}{\partial x}, \theta\left(\eta\right) = \dfrac{T-T_\infty}{T_w-T_\infty}, \eta = \dfrac{r^2-a^2}{2q}\left(\dfrac{u_w}{\nu_f}\right)\end{cases} \tag{18}$$

Using Equation (18), the Equation (1) and (2) reduced to Equations (17) and (18)

$$\left(1+2\eta\beta\right)\frac{1}{\varepsilon_1}\left(1+\frac{1}{\delta}\right)f''' + 2\frac{1}{\varepsilon_1}\beta f'' + \left(ff''-f'^2\right) - Kf' + \frac{1}{\varepsilon_3}Ze^{-p\eta} + Gr\theta = 0 \tag{19}$$

$$\frac{\varepsilon_4}{\varepsilon_5}\left(1+2\eta\beta\right)\theta'' + \mathrm{Pr}\left(f\theta'-nf'\theta\right) + \frac{1}{\varepsilon_2\varepsilon_5}Ec\,\mathrm{Pr}\left(1+\frac{1}{\delta}\right)\left(2\eta\beta+1\right)\left(f''\right)^2 + 2\frac{\varepsilon_4}{\varepsilon_5}\beta\theta' + \mathrm{Pr}\left(Af'+B\theta\right) - Ra\theta = 0 \tag{20}$$

The dimensionless boundary condition are [30] , [31] and [2]

$$f(0)=0, f'(0)=1, \theta(0)=1, f'(\infty)\to 0, \theta(\infty)\to 0 \tag{21}$$

In Equations (19) and (20), β is the curvature parameter, δ is the Casson fluid parameter, M is magnetic parmeter, K is the permeability parameter, Z is Hartman number, Gr is the thermal Grashof number, η is the temperature exponent, Ec is the Eckert number and Pr is the Prandtl number are stated below:

$$\beta=\sqrt{\frac{\nu_f l}{a^2 b}},\ M=\frac{\sigma_f B_0^2 x}{\rho_f u_w(x)},\ K=\frac{\nu_f x}{u_w K_p},\ Z=\frac{\pi j_0 M_0 x}{8\rho_f u_w^2},\ Gr=\frac{g\beta_T(T_w-T_\infty)x}{u_w^2},$$

$$\mathrm{Pr}=\frac{\nu_f}{\alpha_f} \tag{22}$$

The physical quantities of interest include drag force, Nusselt number and heat flux have numerous applications in both Engineering and Medical science.
The shearing stress is denoted by:

$$\tau_w=\mu\left(\frac{\partial u}{\partial r}\right)_{r=a} \tag{23}$$

The skin friction coefficient is

$$C_f=\frac{2\tau_w}{\rho u_w^2} \tag{24}$$

$$\text{Therefore, } \frac{1}{2}C_f\,\mathrm{Re}^{\frac{1}{2}}=f''(0) \tag{25}$$

Where $\mathrm{Re}=\frac{lb}{\nu}$ is the Reynolds number.
The heat transfer rate close to the sheet is described as

$$q_w=-\kappa\left(\frac{\partial T}{\partial r}\right)_{r=a} \tag{26}$$

$$Nu_x=\frac{xq_w}{\kappa(T_w-T_\infty)} \tag{27}$$

However,

$$\frac{Nu_x}{\mathrm{Re}^{1/2}}=-\theta'(0) \tag{28}$$

2.1 Numerical Approach

The dimensionless coupled system of ordinary differential Equation (19) -(20) is nonlinear. Therefore, it can be solved by a numerical procedure called Runge-Kutta fourth order scheme with shooting technique alongside. The highly nonlinear system of ordinary differential equations in Equations (19) -(20) is converted to a system of first-order codes as expressed below:

$$f=\chi_1,\ f'=\chi_2,\ f''=\chi_3, \theta=\chi_4, \theta'=\chi_5 \tag{29}$$

$$\chi_2'=\chi_3 \tag{30}$$

$$\chi_3'=\frac{1}{(1+2\eta\beta)}\left(\frac{\delta}{1+\delta}\right)\left(\varepsilon_1 K\chi_2+\varepsilon_1\varepsilon_2 Ze^{-p\eta}+\varepsilon_1 Gr\chi_5-2\beta f\chi_3-\varepsilon_1\left(\chi_1\chi_3-\chi_2^2\right)\right) \tag{31}$$

$$\chi_4'=\chi_5 \tag{32}$$

J. of Science and Technology Vol. 16 No. 1 (2024) p. 10-22

$$\chi_5' = \frac{\varepsilon_5}{\varepsilon_4}\frac{1}{(1+2\eta\beta)}\left[-\Pr(\chi_1\chi_5 - n\chi_2\chi_5) - \frac{1}{\varepsilon_2\varepsilon_5}Ec\Pr\left(1+\frac{1}{\delta}\right)(2\eta\beta+1)(\chi_3)^2 - 2\frac{\varepsilon_4}{\varepsilon_5}\beta\chi_5 - \Pr(A\chi_2 + B\chi_4) + Ra\chi_4\right] \quad (33)$$

Together with the boundary condition:

$$\chi_1(0)=0, \chi_2(0)=1, \chi_4(0)=1, \chi_3(0)=q_1, \chi_4(0)=q_2, \chi_5(0)=q_3 \quad (34)$$

The initial predict values $q_1 q_2$ and q_3 in Equation (29) are carefully chosen and developed such that the free stream conditions are asymptotically satisfied. The values of $q_1 q_2$ and q_3 are approximately calculated by using Newton's technique so that the end points are satisfied at topmost numerical values of η = 8 with error smaller than 10^{-4}.

3. Results and Discussions

Figure 2a depicts the influence of the Hartmann number (Z) on the velocity of the Casson hybrid fluid. It is observed that an increase in the Hartmann number from 0.5 to 1.5 causes a corresponding increase in the fluid flow velocity of approximate value of 0.9 to 1,1. The Hartmann number is dimensionless parameter that result from modified magnetic field that generated (parallel Lorentz force increases), which reduces fluid friction [53]. Thus, the Casson hybrid fluid velocity increases with increasing Z values. The effect of the Casson fluid parameter (β) on fluid velocity is illustrated in Figure 2b. It is observed that an increase in β corresponds to an increase in the shear stress of the fluid and dynamic viscosity that consequently reduces the fluid velocity [51].

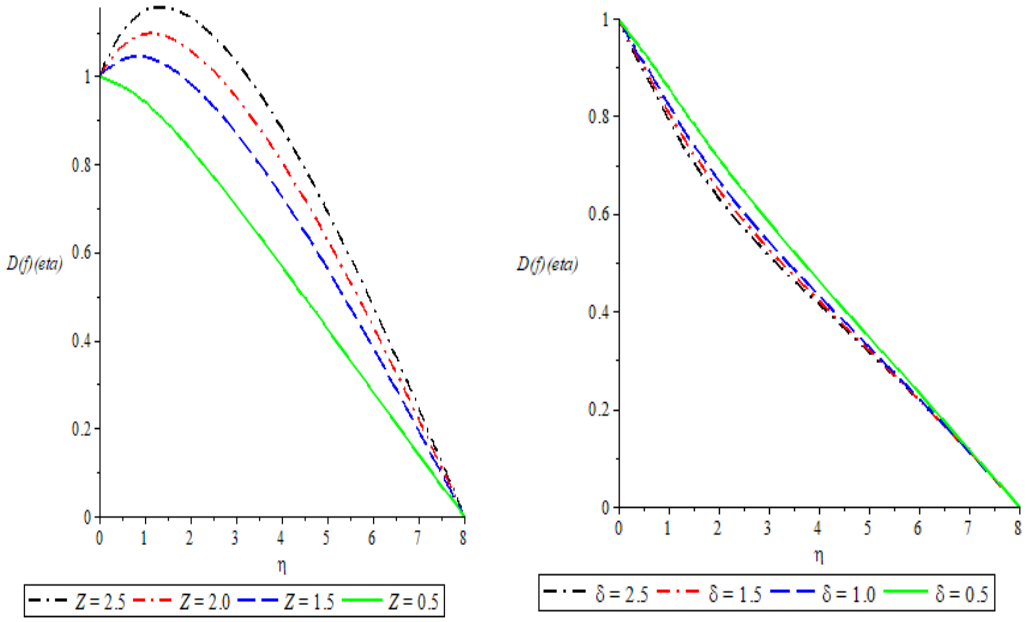

Fig. 2 *(a) Effect of Hartmann number Z on fluid velocity; (b) Effect of various values of Casson Parameter on fluid velocity*

Figure 3a shows that an increase in the value of parameter P declines fluid velocity. An increase in the value of P leads to an increase in the width of the electrode and an increase in the opposing force that decreases the fluid velocity. In figure 3b, an increase in K values decreases the hybrid nanofluid velocity because the presence of void spaces within the medium slows down the fluid. This decline in fluid velocity is due to the blockade of flow paths and the interaction of the fluid with the solid matrix of the medium. Also, the fluid experiences an increase in resistance as it passes through the porous structure, leading to a decrease in velocity compared to what it would be on an open, non-porous surface. In reality, the porosity of vessels invaded by cancerous malignant cells will increase, which leads to a reduction in blood flow.

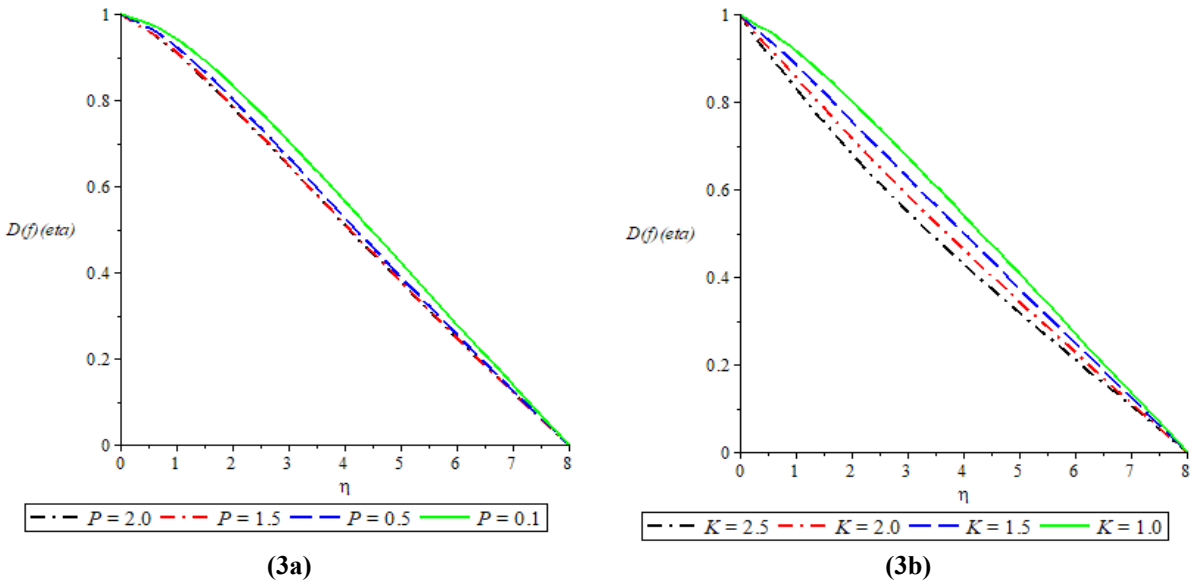

Fig. 3 *(a, b) A plot showing the effect of various values of parameter (P) and Porosity parameter (K)on fluid velocity*

Figures 4a and 4b show that an increase in the values of the space- and temperature-dependent heat source parameters (A and B) leads to an increase in the blood temperature. This temperature increase peaks and then decreases due to heat loss to the surroundings. This behavior is attributed to the increase in the heat flux at the blood surface due to the exponential dependence of the heat source on the temperature, as well as the dissipation to the surrounding. The rise in blood temperature has implications for the success of photothermal therapy in cancer treatment and other medical applications [32].

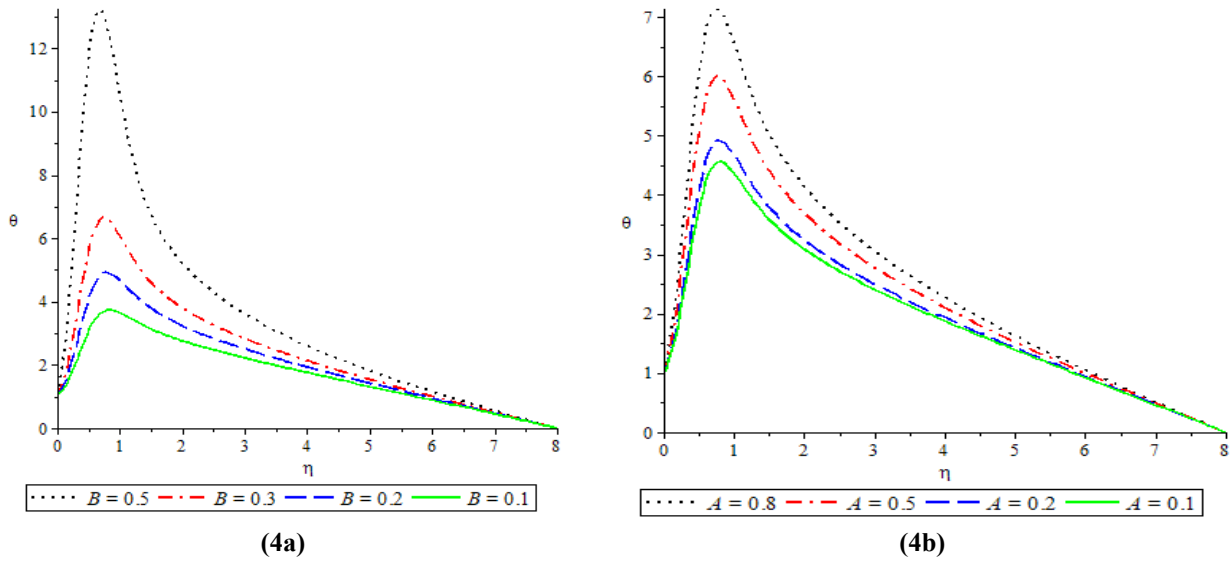

Fig. 4 *(a) Effect of temperature dependent heat generation parameter on temperature; (b) Effect of space dependent heat generation parameter on temperature*

Figure 5a shows that an increase in the values of the radiation parameter (Ra) leads to an increase in the hybrid nanofluid temperature. The temperature rises to a peak and then drops rapidly due to the release of heat to the surroundings as the fluid flows away from the cylinder. This means that the temperature of the biological system can be increased by increasing the radiative heat flux. Figure 5b depicts the effect of various values of the Eckert number (Ec) on the fluid temperature. Ec is a dimensionless number that shows the relationship between a fluid flow kinetic energy and the boundary layer enthalpy change. It's also used to characterize heat transfer dissipation. It is observed that an increase in Ec leads to an increase in temperature [55].

J. of Science and Technology Vol. 16 No. 1 (2024) p. 10-22

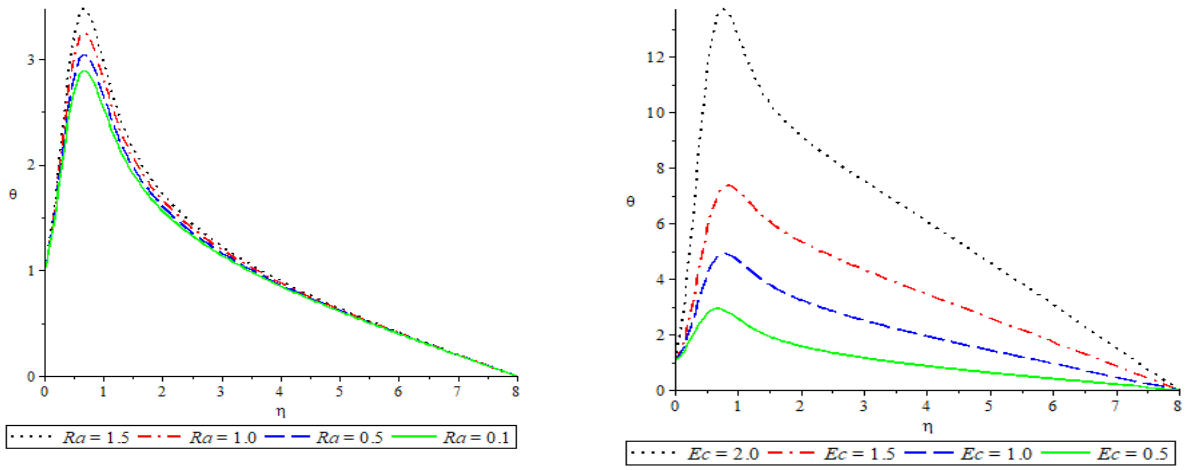

(5a) **(5b)**

Fig. 5 (a, b) *The effect of various values of radiation parameter and of Eckert number of fluid temperature*

As shown in Figure 6a, the fluid velocity profile increases with increasing values of the thermal Grashof number (Gr) from 0.1 to 0.3, there is approximately 50 percent increase in the fluid velocity, but decreases as the distance from the fluid decreases. The thermal Grashof number represents the buoyancy-driven natural convection in a fluid. As the buoyancy force increases, the friction force of the fluid decreases, which in turn increases the fluid velocity. It is seen from Figure 6b that an increase in the curvature parameter enhances the fluid temperature. As the value of increases, the radius of the cylinder decreases curvature helps to enhance the heat transfer.

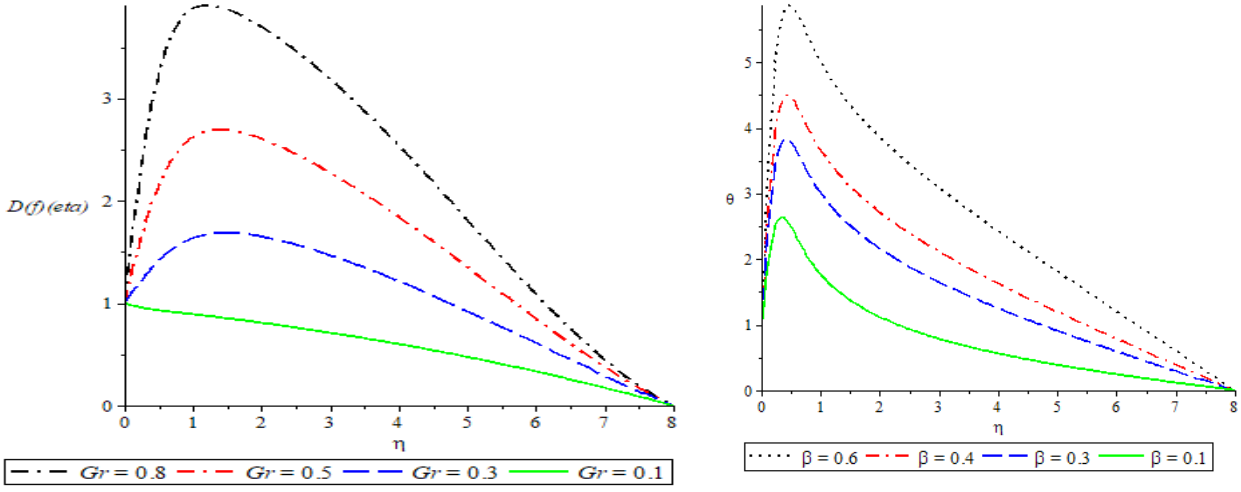

(6a) **(6b)**

Fig. 6 *(a, b) Shows the effect of Grashof number Gr Velocity and Curvature parameter (β) on fluid temperature*

4. Conclusion

In this comprehensive study, we have meticulously analyzed the complex interplay of modified magnetic fields, non-uniform heat sources/sinks, and thermal radiation in the context of Casson hybrid nanofluid flow through a stretching cylinder. Furthermore, we have incorporated the crucial factors of internal heat generation and radiation effects into our investigation. Through the adept utilization of the fourth-order RKF method and the shooting approach with the aid of Maple 18.0 software, we have successfully tackled the transformed model equations. The implications of our study are profound and can be summarized as follows:

i. Enhanced Momentum Fields (Z): Our research reveals that the momentum fields exhibit a significant enhancement for larger values of Z. This finding underscores the pivotal role that modified magnetic fields play in amplifying the flow characteristics within the system.

ii. Temperature Augmentation (Ec and Ra): Higher values of the Eckert number (Ec) and radiation parameter (Ra) have a notable impact on temperature. They lead to an increase in temperature within

the system, shedding light on the intricate relationship between heat transfer and radiation effects in nanofluid dynamics. 3. Casson Fluid Parameter Influence: It is evident from our study that both the temperature and velocity of the fluid experience a decline as the values of the Casson fluid parameter increase. This observation highlights the non-linear behavior of Casson fluids and their effect on the thermal and flow characteristics.

iii. Permeability Parameter (K): Notably, our investigation reveals an intriguing phenomenon - opposite movement is observed for larger values of the permeability parameter (K). This counterintuitive result emphasizes the importance of considering permeability in nanofluid flow scenarios and its influence on the overall flow patterns.

In conclusion, our research provides valuable insights into the intricate dynamics of Casson hybrid nanofluid flow through a stretching cylinder, considering a multitude of factors. These findings have the potential to inform and advance application in the treatment of cancer.

Nomenclatures

u, v	Fluid velocity in x and r direction
ρ_f	Fluid density
ρ_{s1}	Density of the Hybrid nanoparticle MoS_2
ρ_{s2}	Density of the Hybrid nanoparticle SiO_2
μ_{hnf}	Dynamic viscosity of hybrid nanofluid
μ_f	Dynamic viscosity of fluid
δ	Casson fluid parameter
β	Curvature Parameter
$B_\circ$	Applied magnetic induction
g	Acceleration due to gravity
j_0	Current density
M_0	Magnetization of the Magnet
β_T	Thermal expansion coefficient
T	Fluid temperature
T_∞	Free stream temperature
σ_{hnf}	Electrical conductivity of the Hybrid Nanofluid
σ_1	Electrical conductivity of the Hybrid Nanoparticle
σ_2	Electrical conductivity of the Hybrid Nanoparticle
b	Characteristic velocity
L	Reference length
U_w	Reference velocity
ν_{hnf}	Kinematic viscosity hybrid nanofluids
f	Velocity profile
η	Similarity variable
θ	Temperature profile
	Concentration profile
C_p	Particles heat capacity to fluid at Constant pressure
σ	Electrical conductivity of the surface temperature
a	Length of the electrode
T_w	Wall temperature
ψ	Stream function

M	Magnetic Parameter
F_s	Forchheimer parameter
K	Porosity parameter
G_r	Thermal Grashof number
φ_1	Volume fraction of nano particle solid Ra
φ_2	Volume fraction of nanoparticle solid AL_2O_3
E_c	Eckert number
P_r	Prandtl number

Acknowledgment

The authors gratefully acknowledge the support provided by the Department of Pure and Applied Mathematics at Ladoke Akintola University of Technology, Ogbomoso, Nigeria.

Conflict of Interest

The authors confirm that there is no potential conflict of interest involved in the research, the authoring, or the publication of this article

Author Contributions

A.A, S.O.O, A.O.A, M.O.A, A.O.A*: conceptualized the research,* ***A.A, S.O.O, A.O.A, M.O.A, A.O.A*** *drafted the manuscript, reviewed it while* ***A.A, S.O.O*** *wrote its final version.*

References

[1] Adun, H., Kavaz, D., & Dagbasi, M. (2021). Review of ternary hybrid nanofluid: Synthesis, stability, thermophysical properties, heat transfer applications, and environmental effects. Journal of Cleaner Production, 328, 129525.
[2] Das, P. K. (2017). A review based on the effect and mechanism of thermal conductivity of normal nanofluids and hybrid nanofluids. Journal of Molecular Liquids, 240, 420-446.
[3] Yang, L., Ji, W., Mao, M., & Huang, J. N. (2020). An updated review on the properties, fabrication and application of hybrid-nanofluids along with their environmental effects. Journal of Cleaner Production, 257, 120408.
[4] Alfellag, M. A., Kamar, H. M., Sidik, N. A. C., Muhsan, A. S., Kazi, S. N., Alawi, O. A., & Abidin, U. (2023). Rheological and thermophysical properties of hybrid nanofluids and their application in flat-plate solar collectors: a comprehensive review. Journal of Thermal Analysis and Calorimetry, 148(14), 6645-6686.
[5] Yasmin, H., Giwa, S. O., Noor, S., & Sharifpur, M. (2023). Experimental exploration of hybrid nanofluids as energy-efficient fluids in solar and thermal energy storage applications. Nanomaterials, 13(2), 278.
[6] Ramzan, M., Javed, M., Rehman, S., Ahmed, D., Saeed, A., & Kumam, P. (2022). Computational assessment of microrotation and buoyancy effects on the stagnation point flow of carreau–yasuda hybrid nanofluid with chemical reaction past a convectively heated riga plate. ACS omega, 7(34), 30297-30312.
[7] Khashi'ie, N. S., Md Arifin, N., & Pop, I. (2020). Mixed convective stagnation point flow towards a vertical Riga plate in hybrid Cu-Al2O3/water nanofluid. Mathematics, 8(6), 912.
[8] Sarkar, S., kumar Pal, T., Ali, A., & Das, S. (2022). Themo-bioconvection of gyrotactic microorganisms in a polymer solution near a perforated Riga plate immersed in a DF medium involving heat radiation, and Arrhenius kinetics. Chemical Physics Letters, 797, 139557.
[9] Nasir, S., Berrouk, A., & Khan, Z. (2024). Efficiency assessment of thermal radiation utilizing flow of advanced nanocomposites on riga plate. Applied Thermal Engineering, 242, 122531.
[10] Nadeem, M., Siddique, I., Bilal, M., & Ali, R. (2022). Significance of heat transfer for second-grade fuzzy hybrid nanofluid flow past over a stretching/shrinking riga wedge.
[11] Ali, H. M., Rehman, T. U., Arıcı, M., Said, Z., Duraković, B., Mohammed, H. I., ... & Teggar, M. (2024). Advances in thermal energy storage: Fundamentals and applications. Progress in Energy and Combustion Science, 100, 101109.
[12] Zhang, Z. M., Zhang, Z. M., & Luby. (2007). Nano/microscale heat transfer (Vol. 410). New York: McGraw-Hill.

[13] Paul, A., & Das, T. K. (2023). Darcy–Forchheimer MHD radiative flow through a porous space incorporating viscous dissipation, heat source, and chemical reaction effect across an exponentially stretched surface. Heat Transfer, 52(1), 807-825.
[14] Swain, L., Sharma, R. P., & Mishra, S. R. (2024). Illustration of thermal radiation on the flow analysis of hybrid nanofluid within an expanding/contracting channel. Modern Physics Letters B, 38(11), 2450072.
[15] Vyas, P., & Srivastava, N. (2013). On dissipative radiative MHD boundary layer flow in a porous medium over a non isothermal stretching sheet. Journal of Applied Fluid Mechanics, 5(4), 23-31.
[16] Prasanth, B. K., Alkhowaiter, S., Sawarkar, G., Dharshini, B. D., Baskaran, A. R., Prasanth, K., ... & Baskaran, A. R. (2023). Unlocking Early Cancer Detection: Exploring Biomarkers, Circulating DNA, and Innovative Technological Approaches. Cureus, 15(12).
[17] Panda, P., Mishra, S. S., & Pati, K. C. (2014). NANO MEDICINE: AN EMERGING TREND IN MOLECULAR DELIVERY. Journal of Drug Delivery and Therapeutics, 98-106.
[18] Kumar, D. D., & Arasu, A. V. (2018). A comprehensive review of preparation, characterization, properties and stability of hybrid nanofluids. Renewable and Sustainable Energy Reviews, 81, 1669-1689.
[19 Park, J. H., von Maltzahn, G., Ruoslahti, E., Bhatia, S. N., & Sailor, M. J. (2008). Micellar hybrid nanoparticles for simultaneous magnetofluorescent imaging and drug delivery. *Angewandte Chemie*, *120*(38), 7394-7398.
[20] Zhou, L., Yuan, J., & Wei, Y. (2011). Core–shell structural iron oxide hybrid nanoparticles: from controlled synthesis to biomedical applications. *Journal of materials chemistry*, *21*(9), 2823-2840.
[21] Ahmad, S., Akhter, S., Shahid, M. I., Ali, K., Akhtar, M., & Ashraf, M. (2022). Novel thermal aspects of hybrid nanofluid flow comprising of manganese zinc ferrite MnZnFe2O4, nickel zinc ferrite NiZnFe2O4 and motile microorganisms. *Ain Shams Engineering Journal*, *13*(5), 101668.
[22] Jun, Y. W., Seo, J. W., & Cheon, J. (2008). Nanoscaling laws of magnetic nanoparticles and their applicabilities in biomedical sciences. *Accounts of chemical research*, *41*(2), 179-189.
[23] Soares, D. C. F., Domingues, S. C., Viana, D. B., & Tebaldi, M. L. (2020). Polymer-hybrid nanoparticles: Current advances in biomedical applications. *Biomedicine & Pharmacotherapy*, *131*, 110695.
[24] Tripathi, J., Vasu, B., Bég, O. A., & Gorla, R. S. R. (2021). Unsteady hybrid nanoparticle-mediated magneto-hemodynamics and heat transfer through an overlapped stenotic artery: Biomedical drug delivery simulation. *Proceedings of the Institution of Mechanical Engineers, Part H: Journal of Engineering in Medicine*, *235*(10), 1175-1196.
[25] Bhatti, M. M., & Abdelsalam, S. I. (2021). Bio-inspired peristaltic propulsion of hybrid nanofluid flow with Tantalum (Ta) and Gold (Au) nanoparticles under magnetic effects. *Waves in Random and Complex Media*, 1-26.
[26] Chahregh, H. S., & Dinarvand, S. (2020). TiO2-Ag/blood hybrid nanofluid flow through an artery with applications of drug delivery and blood circulation in the respiratory system. *International Journal of Numerical Methods for Heat & Fluid Flow*.
[27] Alghamdi, W., Alsubie, A., Kumam, P., Saeed, A., & Gul, T. (2021). MHD hybrid nanofluid flow comprising the medication through a blood artery. *Scientific Reports*, *11*(1), 1-13.
[28] Jawad, M., Khan, Z., Bonyah, E., & Jan, R. (2022). Analysis of hybrid nanofluid stagnation point flow over a stretching surface with melting heat transfer. *Mathematical Problems in Engineering*, *2022*. https://www.hindawi.com/journals/mpe/2022/9469164/
[29] Awais, M., Shah, Z., Perveen, N., Ali, A., Kumam, P., Rehman, H. U., & Thounthong, P. (2020). MHD effects on ciliary-induced peristaltic flow coatings with rheological hybrid nanofluid. *Coatings*, *10*(2), 186.
[30] Reddy, S. R. R., Raju, C. S. K., Gunakala, S. R., Basha, H. T., & Yook, S. J. (2022). Bio-magnetic pulsatile CuO–Fe3O4 hybrid nanofluid flow in a vertical irregular channel in a suspension of body acceleration. *International Communications in Heat and Mass Transfer*, *135*, 106151.s
[31] Reddy, P. B. A. (2020). Biomedical aspects of entropy generation on electromagnetohydrodynamic blood flow of hybrid nanofluid with nonlinear thermal radiation and non-uniform heat source/sink. *The European Physical Journal Plus*, *135*, 1-30.
[32] Puneeth, V., Manjunatha, S., Makinde, O. D., & Gireesha, B. J. (2021). Bioconvection of a radiating hybrid nanofluid past a thin needle in the presence of heterogeneous–homogeneous chemical reaction. Journal of Heat Transfer, 143(4).
[33] Imran, M., Yasmin, S., Waqas, H., Khan, S. A., Muhammad, T., Alshammari, N., ... & Khan, I. (2022). Computational analysis of nanoparticle shapes on hybrid nanofluid flow due to flat horizontal plate via solar collector. *Nanomaterials*, *12*(4), 663.
[34] Li, F., Soomro, F. A., & Imtiaz, J. (2021). Influences of imposed magnetic force on treatment of hybrid nanofluid involving non-Darcy porous model. *International Communications in Heat and Mass Transfer*, *125*, 105318
[36] Waqas, H., Manzoor, U., Shah, Z., Arif, M., & Shutaywi, M. (2021). Magneto-burgers nanofluid stratified flow with swimming motile microorganisms and dual variables conductivity configured by a stretching cylinder/plate. *Mathematical Problems in Engineering*, *2021*, 1-16

[37] Cogley ACL, Vincenti WG, Giles ES. Differential approximation for radiative heat transfer in a non-grey gasnear equilibrium. Am Instit Aeronaut Astronaut. 1968;6(3):551-553.
[38] Reddy, Y. D., Goud, B. S., Nisar, K. S., Alshahrani, B., Mahmoud, M., & Park, C. (2023). Heat absorption/generation effect on MHD heat transfer fluid flow along a stretching cylinder with a porous medium. *Alexandria Engineering Journal*, *64*, 659-666.
[39] Ishak, A., Nazar, R., & Pop, I. (2008). Magnetohydrodynamic (MHD) flow and heat transfer due to a stretching cylinder. *Energy Conversion and Management*, *49*(11), 3265-3269.
[40] Swain, B. K., Parida, B. C., Kar, S., & Senapati, N. (2020). Viscous dissipation and joule heating effect on MHD flow and heat transfer past a stretching sheet embedded in a porous medium. *Heliyon*, *6*(10).
[41] Ullah, I., Alkanhal, T. A., Shafie, S., Nisar, K. S., Khan, I., & Makinde, O. D. (2019). MHD slip flow of Casson fluid along a nonlinear permeable stretching cylinder saturated in a porous medium with chemical reaction, viscous dissipation, and heat generation/absorption. *Symmetry*, *11*(4), 531.
[42] Vajravelu, K., Prasad, K. V., & Santhi, S. R. (2012). Axisymmetric magneto-hydrodynamic (MHD) flow and heat transfer at a non-isothermal stretching cylinder. *Applied Mathematics and computation*, *219*(8), 3993-4005.
[43] Abbas, Z., Majeed, A., & Javed, T. (2013). Thermal radiation effects on MHD flow over a stretching cylinder in a porous medium. *Heat Transfer Research*, *44*(8).
[44] Saeed, A., Alsubie, A., Kumam, P., Nasir, S., Gul, T., & Kumam, W. (2021). Blood based hybrid nanofluid flow together with electromagnetic field and couple stresses. *Scientific Reports*, *11*(1), 12865.
[45] Gul, T., Qadeer, A., Alghamdi, W., Saeed, A., Mukhtar, S., & Jawad, M. (2021). Irreversibility analysis of the couple stress hybrid nanofluid flow under the effect of electromagnetic field. *International Journal of Numerical Methods for Heat & Fluid Flow*, *32*(2), 642-659.
[46] Gul, T., Ali, B., Alghamdi, W., Nasir, S., Saeed, A., Kumam, P., ... & Jawad, M. (2021). Mixed convection stagnation point flow of the blood-based hybrid nanofluid around a rotating sphere. *Scientific Reports*, *11*(1), 7460.
[47] Saeed, A., Khan, N., Gul, T., Kumam, W., Alghamdi, W., & Kumam, P. (2021). The flow of blood-based hybrid nanofluids with couple stresses by the convergent and divergent channel for the applications of drug delivery. *Molecules*, *26*(21), 6330.
[48] Ramzan, M., Shah, Z., Kumam, P., Khan, W., Watthayu, W., & Kumam, W. (2022). Bidirectional flow of MHD nanofluid with Hall current and Cattaneo-Christove heat flux toward the stretching surface. *Plos one*, *17*(4), e0264208.
[49] Ramzan, M. (2015). Influence of Newtonian heating on three dimensional MHD flow of couple stress Panda, P., Mishra, S. S., & Pati, K. C. (2014). NANO MEDICINE: AN EMERGING TREND IN MOLECULAR DELIVERY. Journal of Drug Delivery and Therapeutics, 98-106.nanofluid with viscous dissipation and joule heating. *PloS one*, *10*(4), e0124699.
[50] Khan, M. I., Tamoor, M., Hayat, T., & Alsaedi, A. (2017). MHD boundary layer thermal slip flow by nonlinearly stretching cylinder with suction/blowing and radiation. *Results in Physics*, *7*, 1207-1211.
[51] Malik, M. Y., Salahuddin, T., Hussain, A., & Bilal, S. (2015). MHD flow of tangent hyperbolic fluid over a stretching cylinder: Using Keller box method. *Journal of magnetism and magnetic materials*, *395*, 271-276.
[52] Eldabe, N. T. M. & Salwa, M. G. E(1995).Heat transfer of MHD non-Newtonian Casson fluid flow between two rotating cylinders. *J.Phys. Soc. Jpn.* **64**, 41–64.
[53] Upreti, H., Pandey, A. K., Joshi, N., & Makinde, O. D. (2023). Thermodynamics and heat transfer analysis of magnetized Casson hybrid nanofluid flow via a Riga plate with thermal radiation. Journal of Computational Biophysics and Chemistry, 22(03), 321-334.
[54] Afzal, S., Qayyum, M., Riaz, M. B., & Wojciechowski, A. (2023). Modeling and simulation of blood flow under the influence of radioactive materials having slip with MHD and nonlinear mixed convection. *Alexandria Engineering Journal*, *69*, 9-24.
[55] Ullah, I., Alkanhal, T. A., Shafie, S., Nisar, K. S., Khan, I., & Makinde, O. D. (2019). MHD slip flow of Casson fluid along a nonlinear permeable stretching cylinder saturated in a porous medium with chemical reaction, viscous dissipation, and heat generation/absorption. Symmetry, 11(4), 531.